Plant–herbivore interactions mediated by plant toxicity

Zhilan Feng[a], Rongsong Liu[a], Donald L. DeAngelis[b,c,*]

[a] *Department of Mathematics, Purdue University, West Lafayette, IN 47907, United States*
[b] *US Geological Survey, University of Miami, Coral Gables, FL 33124, United States*
[c] *Department of Biology, University of Miami, P. O. Box 249118, Coral Gables, FL 33124, United States*

Abstract

We explore the impact of plant toxicity on the dynamics of a plant–herbivore interaction, such as that of a mammalian browser and its plant forage species, by studying a mathematical model that includes a toxin-determined functional response. In this functional response, the traditional Holling Type 2 response is modified to include the negative effect of toxin on herbivore growth, which can overwhelm the positive effect of biomass ingestion at sufficiently high plant toxicant concentrations. Two types of consumption decisions of the herbivore are considered. One of these (Case 1) incorporates the adaptation of the herbivore to control its rate of consumption of plant items when that is likely to lead to levels of toxicity that more than offset the marginal gain to the herbivore of consuming more plant biomass, while the other (Case 2) simply assumes that, although the herbivore's rate of ingestion of plant biomass is negatively affected by increasing ingestion of toxicant relative to the load it can safely deal with, the herbivore is not able to prevent detrimental or even lethal levels of toxicant intake. A primary result of this work is that these differences in behavior lead to dramatically different outcomes, summarized in bifurcation diagrams. In Case 2, a wide variety of dynamics may occur due to the interplay of Holling Type 2 dynamics and the effect of the plant toxicant. These dynamics include the occurrence of bistability, in which both a periodic solution and the herbivore-extinction equilibrium are attractors, as well the possibility of a homoclinic bifurcation. Whether the herbivore goes to extinction in the bistable case depends on initial conditions of herbivore and plant biomasses. For relatively low herbivore resource acquisition rates, the toxicant effect increases the likelihood of 'paradox of enrichment' type limit cycle oscillations, but at higher resource acquisition rates, the toxicant may decrease the likelihood of these cycles.
© 2007 Elsevier Inc. All rights reserved.

Keywords: Plant–herbivore; Chemical defense; Plant toxicity; Bifurcation diagram; Limit cycle; Extinction

1. Introduction

Plants defend themselves against consumption by herbivores through a variety of secondary chemicals that are toxic to herbivores, or decrease their ability to digest plant biomass. This has consequences for the dynamics of plant–herbivore interaction. Chemically-mediated interactions between plants and herbivores have been shown to play an important role in ecology, evolutionary biology, and resource management (e.g., see Bryant et al. (1983, 1992, 1994), Coley et al. (1985), Palo and Robbins (1991), Rosenthal and Berenbaum (1992) and Villalba et al. (2002)). Although recent research indicates that a large part of the explanation for why 'the world is green' involves the top–down control of predators on herbivores (e.g., Terborgh et al. (2006)), defensive chemicals clearly play a role both in directly limiting the amount of plant biomass consumed and indirectly reducing it by inflicting higher mortality and lower growth and reproduction on herbivores (e.g., Murdoch (1966)).

Besides limiting plant consumption, chemical defenses may have implications for the 'paradox of enrichment' (Rosenzweig, 1971), which predicts that increasing plant carrying capacity can lead to destabilization of plant–consumer interactions under certain conditions, leading to limit cycle oscillations. Limit cycles can arise in consumer–resource interactions with a Holling Type 2 functional response (Holling, 1959a,b), because with that saturating response the per capita prey feeding rate of the consumer population decreases with

* Corresponding author at: Department of Biology, University of Miami, P. O. Box 249118, Coral Gables, FL 33124, United States.

E-mail address: ddeangelis@bio.miami.edu (D.L. DeAngelis).
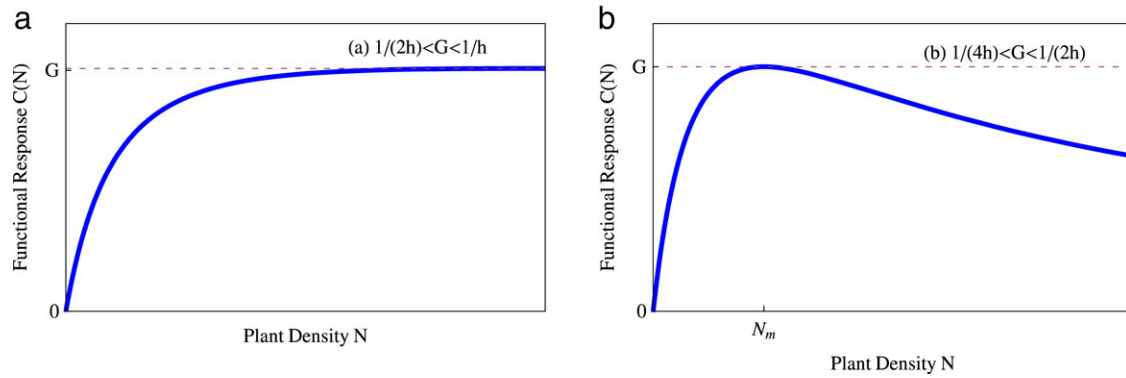
Fig. 1. Graphs of the functional response $C(N)$. (a) $C(N)$ is monotonically increasing. (b) $C(N)$ is unimodal and reaches its maximum at $N_m = \frac{2G}{e\sigma_0(1-2hG)}$.

increasing plant density. The effect of the toxicant could be similar, if in effect it imposes additional resource handling time on the herbivore. On the other hand, if toxicants can decrease the herbivore ability to graze plants to low levels, it is also intuitively possible that the likelihood of such limit cycles could be reduced.

Many other patterns of plant–herbivore interactions, at the population, community, and ecosystem levels, are affected by plant chemical defenses. For this reason, it is important to understand theoretically the sort of effects that can be expected. However, prior models have not explicitly incorporated toxicity effects on the dynamics of mammalian herbivores and plants. To do this we have formulated a functional response that incorporates the occurrence of a toxicant in a plant that, above certain levels of intake by the herbivore, can have a negative effect on herbivore growth. Unlike all previous functional response models of plant–mammal interactions (e.g., Abrams (1989), Lundberg (1988), Lundberg and Astrom (1990) and Spalinger et al. (1988)), our model explicitly incorporates reduction in herbivore growth by toxins. We do not attempt to model the detailed mechanisms of the toxicant's effect on the herbivore, but simply postulate a negative influence in the functional response of the herbivore that increases with toxicant intake. Justification for the function used are given in the discussion and an appendix in the online version of this paper.

The functional response used here is

$$C(N) = f(N)\left(1 - \frac{Tf(N)}{M}\right), \qquad (1)$$

which was originally formulated by Li et al. (2006). This functional response contains two factors. The first factor is the traditional functional response, representing ingestion per unit time, derived on the basis of search by the consumer moving at a constant speed through a space with randomly distributed prey of biomass density N, which may be a Holling Type 2; i.e.,

$$f(N) = \frac{e\sigma N}{1 + he\sigma N}. \qquad (2)$$

The parameter e in Eq. (2) is the resource encounter rate, which depends on the movement velocity of the consumer and its radius of detection of food items. The parameter σ ($0 < \sigma \leq 1$) is the fraction of food items encountered that the herbivore

ingests, while h is the handling time for each prey item, which incorporates the time required for the digestive tract to handle the item.

The second factor in (1), which accounts for the negative effect of toxin, is

$$1 - \frac{Tf(N)}{M} \quad \text{or} \quad 1 - \frac{f(N)}{4G},$$

where $G = M/(4T)$. The parameter M is a measure of the maximum amount of toxicant per unit time that the herbivore can tolerate, T is the amount of toxicant per unit plant biomass, and the factor 4 simplifies the peak value of $C(N)$ (see Eq. (4)). Therefore, the smaller the value of G, the larger the effect the toxin has on the herbivores.

The fraction of encountered resources ingested, σ, is one of the parameters that we will adjust. If σ is assumed to be constant, then when $1/(2h) < G < 1/h$, $C(N)$ is monotone increasing with N, reaching an asymptote (see Fig. 1(a)). Over a range of smaller values of G, $1/(4h) < G < 1/(2h)$, $C(N)$ is unimodal, declining to an asymptote after reaching a peak,

$$C(N_m) = G, \quad \text{at } N_m, \text{ where } N_m = \frac{G}{e\sigma(1/2 - hG)}. \qquad (3)$$

(See Fig. 1(b)). This decrease in $C(N)$ is the result of the increasing negative effect of plant toxicant, which affects the herbivore physiologically, decreasing its ingestion rate.

We will consider two possible behavioral actions by the herbivore under the condition of high plant density ($N > N_m$). In the first, Case 1, the herbivores are able to avoid further consumption beyond the optimal rate of G, for any value of $N > N_m$. Because ingestion of biomass could occur at levels high enough to be damaging, it is reasonable that some animals can adjust their rates of ingestion by controlling the parameter σ when resource encounter rates are high (e.g., see Provenza et al. (2003) and Marsh et al. (2007)). Ingestion is controlled through this parameter, which can be called the 'consumption choice coefficient'. We expect that

$$\sigma \propto N_m/N \qquad (4)$$

when $N > N_m$, as that would effectively 'freeze' $C(N)$ at its maximum value.

Therefore, we write $C(N)$ as $C(N, \sigma)$. A function that has this property is

$$\sigma(N) = \begin{cases} \sigma_0 & \text{for } N \leq N_m \\ \sigma_0 \dfrac{N_m}{N} & \text{for } N_m < N \leq K, \end{cases} \qquad (5)$$

where $\sigma_0 > 0$ is a constant. Let $C_1(N)$ be the corresponding function for the non-constant $\sigma(N)$ given in Eq. (5); i.e.,

$$C_1(N) = \begin{cases} C(N, \sigma_0) & \text{for } N \leq N_m \\ G & \text{for } N > N_m. \end{cases} \qquad (6)$$

In the second behavior, Case 2, the herbivore is assumed unable to control its consumption rate. Therefore, when the herbivore is in an environment where plant density is high, or on the 'descending limb' of the $C(N)$ curve (or $N > N_m$), it consumes to the point where there is a negative effect on ingestion and growth due to detrimental physiological effects of the toxicant. Although this physiological state leads to decreased toxicant ingestion, our assumption is that the herbivore's weakened state is chronic, because any improvement in health would lead again to a temporary higher ingestion rate and then a return to the weakened state.

Our goal is to study these two cases and compare them with the pure Holling Type 2 functional response within the Rosenzweig–MacArthur (RM) model

$$\frac{dN}{dt} = rN \left(1 - \frac{N}{K}\right) - f(N)P, \qquad (7a)$$

$$\frac{dP}{dt} = Bf(N)P - dP, \qquad (7b)$$

where $f(N)$ is given by Eq. (2), the plant grows logistically, and d is herbivore mortality. The dynamics of the RM model are well known. It is known to be necessary that

$$N^* = \frac{d}{e\sigma(B - hd)} < K \qquad (8)$$

for the herbivore to be able to have a non-zero equilibrium, and that

$$d_c = \frac{B}{h} \left(\frac{he\sigma K - 1}{he\sigma K + 1}\right) \qquad (9)$$

is the Hopf bifurcation point, beyond which (e.g., for smaller values of d) limit cycle oscillations occur. In the case of the RM, such changes in behavior are often studied along one or two axes of a parameter space. As our main interest in this study is to explore the joint effect of the plant toxin and herbivore browsing on the outcomes of the plant–herbivore interaction, our analysis is performed using two key parameters, G and $w = BG - d$. The former is a measure of the capacity of the herbivore to tolerate the plant toxicant, per unit toxicant supplied by the ingested plant. The latter represents the maximum possible energy intake by the herbivore, minus loss to mortality, and so is a measure of maximum individual fitness.

Table 1
Definition of parameters used in the Model (10a)–(10c)

	Definition
r	Intrinsic growth rate of plant
T	Amount of toxin contained per unit plant
M	Max amount of toxin a herbivore can consume per unit time
G	$M/4T$
h	Time for handling one unit of plant
e	Rate of encounter per unit plant
σ	Fraction of food items encountered that the herbivore ingest
B	Conversion constant (herbivore biomass per unit of plant)
K	Carry capacity of plant
d	Per capital death rate of herbivore unrelated to plant toxicity

2. Analysis of the toxin-determined functional response model

A model using a functional response similar to (1) with two plant species and one herbivore population was analyzed in Li et al. (2006). In that paper, the factor σ was not considered, and the analysis was conducted only for the case when G is in the interval $(1/2h, 1/h)$ in which $C(N)$ is monotone increasing. In the present paper, we consider the case when G is in the interval $(1/4h, 1/2h)$ in which the function $C(N)$ is unimodal for constant σ. We also allow for the possibility that σ is a function of plant density N with the property specified in Eq. (6). For the analysis presented in this paper, we focus on a model that includes only one plant species and one herbivore population. This will allow us to explore in more detail the new dynamical behavior of the toxin-determined functional response model (TDFRM) for two cases;

(1) when $C(N)$ is constant after reaching its maximum due to the dependence of σ on N, and
(2) when $C(N)$ is unimodal (in which case σ is independent of N).

2.1. The two-dimensional TDFRM

Let $N = N(t)$ and $P = P(t)$ denote the densities of plant and herbivore biomasses at time t. Then the two-dimensional TDFRM is described by the following equations:

$$\frac{dN}{dt} = rN \left(1 - \frac{N}{K}\right) - C(N)P, \qquad (10a)$$

$$\frac{dP}{dt} = BC(N)P - dP, \qquad (10b)$$

$$C(N) = f(N) \left(1 - \frac{f(N)}{4G}\right), \qquad (10c)$$

where $f(N)$ is given in Eq. (2). B is the conversion of consumed plant biomass into new herbivore biomass (through both growth and reproduction), d is the per capita rate of herbivore death due to causes unrelated to plant toxicity, r is the plant intrinsic growth rate, and K is the carrying capacity. All parameters and their units are defined in Table 1.
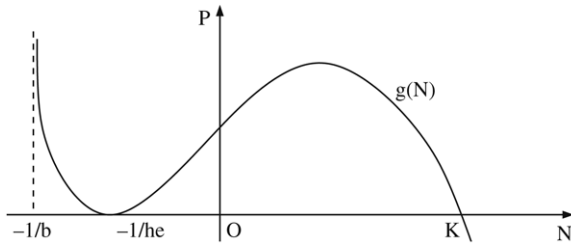
Fig. 2. Plot of the function $g(N)$, which is the N-nullcline that determines interior equilibria. It has a single hump for $N \in (0, K)$.

2.2. Case 1: Dynamics for non-constant $\sigma(N)$

Although it is not difficult to imagine that animals, when encountering food at high levels, may eat to a point that is detrimental to them, as noted above it is also likely that many species are adapted for controlling their rates of ingestion. We consider the case where the herbivore's 'consumption choice function', $\sigma(N)$, that has this property is given in Eq. (5), and the consequent alteration of $C(N)$ to $C_1(N)$ is given in Eq. (6). System (10a)–(10c) with $C_1(N)$ has two boundary equilibria at which $P = 0$:

$$E_0 = (N_0, P_0) = (0, 0), \qquad E_K = (N_K, P_K) = (K, 0).$$

There is one possible interior equilibrium, which we denote by $E^* = (N^*, P^*)$ with $0 < N^* < K$, and $P^* > 0$. For ease of presentation, we rewrite the equation for N (Eq. (10a)) as

$$\frac{dN}{dt} = C(N)\,(g(N) - P) \quad \text{or} \quad \frac{dN}{dt} = C_1(N)(g_1(N) - P) \tag{11}$$

where

$$g(N) = \frac{rN\left(1 - \frac{N}{K}\right)}{C(N)} \quad \text{and} \quad g_1(N) = \frac{rN\left(1 - \frac{N}{K}\right)}{C_1(N)}. \tag{12}$$

For $C(N)$, the zero isocline for dN/dt is (see Fig. 2)

$$P = g(N) = \frac{r(K - N)(1 + he\sigma_0 N)^2}{e\sigma_0 K[1 + e\sigma_0(h - 1/4G)N]} \quad \text{for all } N. \tag{13}$$

For $C_1(N)$, the zero isocline for dN/dt is

$$P = g(N) \quad \text{for } N \le N_m \text{ and } P = g_1(N)$$
$$= \frac{rN(K - N)}{KG} \quad \text{for } N > N_m. \tag{14}$$

2.2.1. Equilibria

The interior equilibrium point $E^* = (N^*, P^*)$ is determined by the intersection of (14) and the zero isocline for $dP/dt = 0$;

$$BC_1(N) = d \quad \text{with } 0 < N^* < K. \tag{15}$$

As stated in the introduction, our analysis takes place in the bifurcation plane defined by parameters G and $w = BG - d$. It can be shown that the interior equilibrium point lies on the (G, w)-plane within the region bounded by

$$\frac{1}{4h} < G < \frac{1}{2h} \qquad 0 < w < BG. \tag{16}$$

We introduce the curve $w_u(G) = BG$ to represent the upper boundary.

The left-hand side of Eq. (15), $BC_1(N)$, cannot exceed BG (see Eq. (6)), which is reached at N_m, so any solution N^* will be bounded, $N^* \le N_m$. The solution N^* can be found by setting the right-hand side of dP/dt equal to 0 to obtain the single solution;

$$N^* = \frac{G(B - 2dh) - \sqrt{\Delta_v}}{2e\sigma_0\left(\frac{B}{4} + dh^2 G - BhG\right)}$$
$$\text{where } \Delta_v = BG(BG - d). \tag{17}$$

The next consideration is whether this solution N^* can occur for values less than K, so that it can be an interior equilibrium point. This involves the question of whether $N_m < K$ or $N_m > K$. N_m is given by Eq. (4), and from that equation it can be shown that $N_m < K$ when

$$G < \frac{e\sigma_0 K}{2(1 + he\sigma_0 K)} \equiv G_c. \tag{18}$$

What this means is that for all $G < G_c$, it is true that $N_m < K$, so that $C(N)$ can attain its maximum value G for values of $N < K$. Let us first focus on the G-axis (along which $w = BG - d = 0$). An equilibrium point can exist on that axis precisely where $N^* = N_m < K$. However, if $G > G_c$, then $N^* < K$ only when

$$BC(K) > d \quad \text{or, what is equivalent, when}$$
$$w \equiv BG - d > B[G - C(K)],$$

since in that case the boundary equilibrium point $(0, K)$ is unstable. To see this more clearly, examine the (G, w) bifurcation plane in Fig. 3. G_c lies along the G-axis ($w = 0$).

Because the G-axis and w-axis are not independent, if one moves from low values to the right along the G-axis, d must increase to maintain $w = 0$. Below the threshold point, G_c, $C(N)$ can always attain a maximum value, G, at N_m, which can satisfy $BG - d = 0$. However, when the threshold value G_c is exceeded, above which $N_m > K$, then, because $C(K)$ cannot exceed G (see Fig. 1(b)), $C(N)$ cannot reach the level G within the domain $(0 < N^* < K)$. Thus, no equilibrium N^* ($<K$) can occur along the G-axis for $G > G_c$. If one moves off the axis in the positive w-direction, by decreasing d, however, a point is reached at which $BC(K) > d = 0$ again. Denote the curve separating the region of space in which the N^* exists from where it does not exist by $w_K(G)$ (see Fig. 3), where

$$w_K(G) = \begin{cases} B[G - C(K)] & \text{for } G > G_c \\ 0 & \text{for } G < G_c \end{cases} \tag{19}$$

for values of $w > w_K(G)$ on the (G, w)-plane, an interior equilibrium exists.

2.2.2. Stability of equilibria and Hopf bifurcation

Two boundary equilibria, E_0 and E_K, exist for all G and w, and stabilities can easily be established for these two equilibria. E_0 is always a saddle point. The Jacobian matrix at $E_K =$
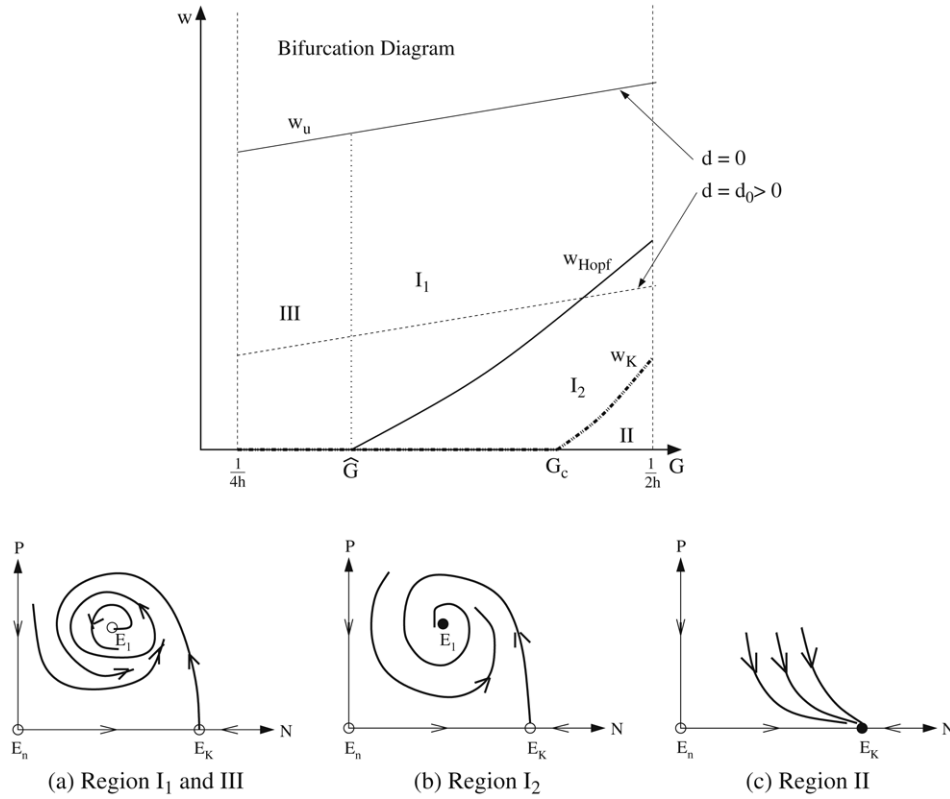
Fig. 3. The top panel shows the bifurcation diagram for Case 1; i.e., where σ is not constant. The axes are G and $w = BG - d$. The bottom panels (a, b, c) are sketches of the phase portraits for (G, w) in various regions. See the text for explanation. The parameter values used are: $r = 0.01$, $K = 1\,700\,000$, $h = 1/200$, $e\sigma_0 = 0.00012$, and $B = 0.00003$ (for the purpose of presentation figures are not drawn to scale).

$(K, 0)$ is

$$J(E_K) = \begin{pmatrix} C_1(K)g'(K) & -C_1(K) \\ 0 & BC_1(K) - d \end{pmatrix},$$

which has two eigenvalues: $\lambda_1 = C_1(K)g'(K)$ and $\lambda_2 = BC_1(K) - d$. From Fig. 2 we know that $g'(K) < 0$ and hence $\lambda_1 < 0$. Therefore, the stability of E_K is determined by the sign of $\lambda_2 = BC_1(K) - d$. Recall that N^* satisfies the equation $BC_1(N^*) - d = 0$. It turns out that the stability of E_K and the existence of E^* are closely related, as briefly noted for four cases, referring to the curve $w_K(G)$ in Fig. 3 (details in Liu et al. (in press)).

(i) $G > G_c$ and $w < w_K$ (Region II in Fig. 3). We know from the discussion above that there is no interior equilibrium. E_K is locally asymptotically stable.

(ii) $G > G_c$ and $w > w_K$ (part of Region I). A unique interior equilibrium exists and E_K is unstable.

(iii) $G < G_c$ and $w < w_K = 0$. There is no interior equilibrium and E_K is locally asymptotically stable.

(iv) $G < G_c$ and $w > w_K = 0$ (Regions I and III). There is a unique interior equilibrium and E_K is unstable.

Now we consider the stability of the interior point $E^* = (N^*, P^*)$. Because it is true that $N \leq N_m$, we have $g_1(N) = g(N)$. The Jacobian matrix at this point is

$$J(E*) = \begin{pmatrix} C(N^*)g'(N^*) & -C(N^*) \\ BC'(N^*)P* & 0 \end{pmatrix}. \qquad (20)$$

Since $C'(N^*) > 0$, it can be shown that the stability of E^* is determined by the sign of $g'(N^*)$ (see Liu et al. (in press)). Let N_g denote the point at which $g(N)$ assumes its maximum. From Fig. 4 we observe that, in the case of $N_g > N_m$, $g'(N^*) > 0$ as $N^* < N_m < N_g$. Hence, E^* is unstable. It can be shown that $N_g = N_m$ if and only if $G = \hat{G}$, where

$$\hat{G} = \frac{e\sigma_0 K}{2(2 + he\sigma_0 K)} < \frac{e\sigma_0 K}{2(1 + he\sigma_2 K)} = G_c.$$

If $G > \hat{G}$ then it follows that $N_g < N_m$, and thus $g'(N^*) = 0$ for a unique $N^* < N_m$. It is shown in Liu et al. (in press) that the equations

$$BC(N^*) - d = 0 \quad \text{and} \quad g'(N^*) = 0 \qquad (21)$$

determine the condition for the Hopf bifurcation in the (G, w)-plane. For example, we can use Eq. (21) to solve for d as a function of G (for $G > \hat{G}$) to get a bifurcation curve in d, which is denoted by

$$
\begin{aligned}
d &= d_{\text{Hopf}}(G) \\
&= \frac{B}{2hG(1 + \rho h)^2} \\
&\quad \times \left[\left(G + \rho hG - \frac{\rho}{4} \right) \left(\frac{5\rho h}{4} - 1 + hG + \rho h^2 G \right) \right] \\
&\quad - \left(G + \rho hG - \frac{3\rho}{4} \right) \sqrt{\Delta_g} \qquad (22)
\end{aligned}
$$

a

b
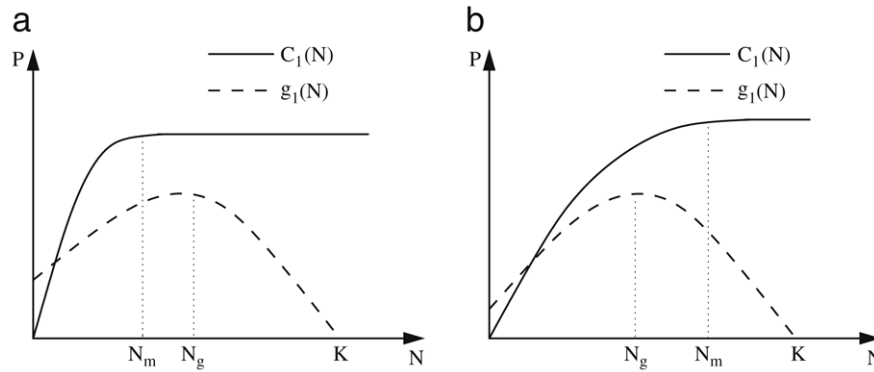
Fig. 4. Graphs of $C_1(N)$ and $g_1(N)$ for establishing stability of the interior point $E^* = (N^*, P^*)$. See the text for explanation.
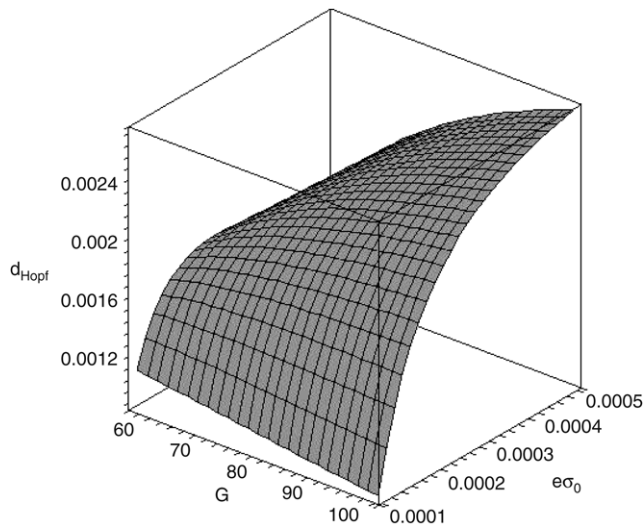
Fig. 5. A Hopf bifurcation surface in terms of the parameter, d, as a function of G and $e\sigma_0$.

where $\Delta_g = h\left(G + \rho hG - \frac{\rho}{4}\right)\left(2 + hG + \rho h^2G - \frac{\rho h}{4}\right)$, $\rho = e\sigma_0 K$.

Then a corresponding Hopf bifurcation curve in the (G, w)-plane will be given by

$$w = w_{\text{Hopf}}(G) \equiv BG - d_{\text{Hopf}}(G).$$

A Hopf bifurcation surface in terms of d, as a function of G and $e\sigma_0$, is plotted in Fig. 5. We can see that, for fixed values of e and σ_0, there is a Hopf bifurcation curve $d = d_{\text{Hopf}}(G)$, which will in turn determine a Hopf bifurcation curve $w = w_{\text{Hopf}}(G)$. It is shown in Liu et al. (in press) that the stability of E^* switches from stable to unstable when w increases and passes the curve w_{Hopf}, and that stable periodic solutions exist for $w > w_{\text{Hopf}}$ (and close to w_{Hopf}).

Notice that the curve $w_{\text{Hopf}}(G)$ intersects $w = 0$ at $\hat{G}$ and that $0 < w_{\text{Hopf}}(G) < BG$ for all G such that $\hat{G} < G < 1/2h$; thus, we can draw the curve as shown in the bifurcation diagram (see Fig. 3). In this bifurcation diagram, the region to the left of the vertical line $G = \hat{G}$ is denoted by III and the region to the right of $G = \hat{G}$ is denoted by I. Thus E^* is always unstable in Region III.

In Region I, $G > \hat{G}$ and $N_g < N_m$. From the analysis above we know that the curve $w_{\text{Hopf}}(G)$ divides Region I into I_1 and

Table 2
Local stability results when σ is not constant

	I_1	I_2	II	III
E_0	Saddle	Saddle	Saddle	Saddle
E^*	Unstable	**Stable**	DNE	Unstable
E_K	Saddle	Saddle	**Stable**	Saddle
PS	**Stable**	DNE	DNE	**Stable**

DNE: does not exist; PS: Periodic solution.

I_2, such that E^* is unstable in I_1 and locally asymptotically stable in I_2 and that a limit cycle exists in Region I_1 (see Fig. 3). These results are summarized in Table 2 and depicted in the bifurcation diagram Fig. 3(a)–(c).

To verify the above analytic results, numerical simulations were performed for the system (10a)–(10c) with $C(N) = C_1(N)$ given by Eq. (6). These are shown in Appendix 1 in the online version of this paper.

The bifurcation diagram displays the interplay of the Holling Type 2 functional response and the 'toxicant' factor, $1 - f(N)/4G$, on the behavior of the model. The upper-right-hand corner of the diagram, where $G \approx 1/2h$ and w is relatively large, is the area of the plane where the toxicant has the least effect on the dynamics (Region I_1). In this region, the system behaves almost like a simple consumer–resource system with a single interior equilibrium point and Holling Type 2 dynamics. The large value of w means that the consumer has a high per capita energy input relative to energy loss (mortality). Therefore, in the sense of the 'paradox of enrichment' (Rosenzweig, 1971), the node is unstable and there is a stable limit cycle around it. If G is held fixed, but w is decreased, this is the same as increasing the mortality rate d. This increase in herbivore mortality tends to stabilize the equilibrium in moving across the Hopf bifurcation line from Region I_1 to I_2, where it becomes a stable node. A sufficient further increase in d (decrease in w), however, causes extinction of the herbivore, as energy intake cannot keep up with losses (Region II).

If we decrease both G and w, but keep d fixed ($d = d_0$), along a diagonal straight line from the middle of the right-hand side of the bifurcation diagram (Fig. 3) towards the lower-left-hand corner, then we can see the effects of G alone on the system behavior. The system undergoes a series of changes leading from dominance of simple Holling Type II dynamics to

dominance by the effect of the toxicant. As G and w decrease, moving from Region I_2 to I_1, the single stable interior point, $E_1^* = (N_1^*, P_1^*)$, becomes unstable, producing a limit cycle.

An interesting aspect is the role that the toxicant effect, G, and the product, $e\sigma_0$, play in the occurrence of the Hopf bifurcation. For the RM model, the Hopf bifurcation occurs at $d = d_c$, given by Eq. (9). For the TDFRM, the Hopf bifurcation occurs at $d = d_{\text{Hopf}}(G)$ (Eq. (22)). We can fix all parameters involved in the expression on the right-hand-side of Eq. (9) and consider the relation between d_c and d_{Hopf}. There are three scenarios depending on the value of $e\sigma_0$. In Fig. 6(a)–(c), the solid curve is $d = d_{\text{Hopf}}(G)$ and the dashed line is d_c. In (a), $d_c > d_{\text{Hopf}}(G)$ for all G, in which case the Hopf bifurcation occurs for smaller d, as compared with the RM model. In (b), $d_c < d_{\text{Hopf}}(G)$ for $G > G_0$ and $d_c > d_{\text{Hopf}}(G)$ for $G < G_0$, where G_0 lies between G_c and $1/4h$, in which case the Hopf bifurcation occurs for larger (smaller) d if G is large (smaller). In (c), $d_c < d_{\text{Hopf}}(G)$ for all G, in which case the Hopf bifurcation occurs for larger d. Thus the toxicant effect appears to be stabilizing for the largest value of $e\sigma_0$ (top panel), as a lower value of d is required to reach the Hopf bifurcation than in the RM model. For the smallest value of $e\sigma_0$ (bottom panel) the opposite is true. It is clear from Fig. 6 that a change in $e\sigma_0$ affects the relative locations of the RM and TDFRM Hopf bifurcations along the d-axis. Now examine more closely the effect of G. Fig. 7 shows that for larger $e\sigma_0$ (left panel), decreasing G can stabilize the system (limit cycle oscillations disappear as G decreases along the constant line $d = d_1$ and passes G_0), whereas for a substantially smaller $e\sigma_0$ (right panel), decreasing G can destabilize the system (limit cycle oscillations appear as G decreases along the constant line $d = d_1$ and passes G_0), similar to what we see moving along the dotted line towards lower values of G in Fig. 3. We offer an explanation for these contrasting behaviors in the Discussion. The bifurcation diagram (Fig. 3) shows only the destabilizing scenario. The stabilizing scenario can occur for higher values of $e\sigma_0$, which change the (G, w)-plane's configuration. Decreasing G also increases the period of the limit cycle (see Appendix 2 in the online version of this paper).

2.3. Case 2. Dynamics for constant $\sigma(N)$

The case that $\sigma(N) = \sigma_0$ for all N means that the herbivore does not deliberately decrease the fraction of encountered prey it ingests; however, for prey densities $N > N_m$ its rate of ingestion is lowered due to physiological stress by the toxin. In this case, our results show that the system exhibits more complex dynamics than Case 1, including both bistability and homoclinic bifurcations. The functions $C(N)$ and $g(N)$ are now given by Eq. (1) and the left-hand term in Eq. (12), respectively, for all values of N. This differs from Case 1, in which $C_1(N) = G$ for $N > N_m$, and it makes a large difference in the dynamics.

2.3.1. Equilibria

The conditions on equilibria in Case 2 are similar to Case 1 for $G > G_c$. For $G < G_c$, however, things are different in
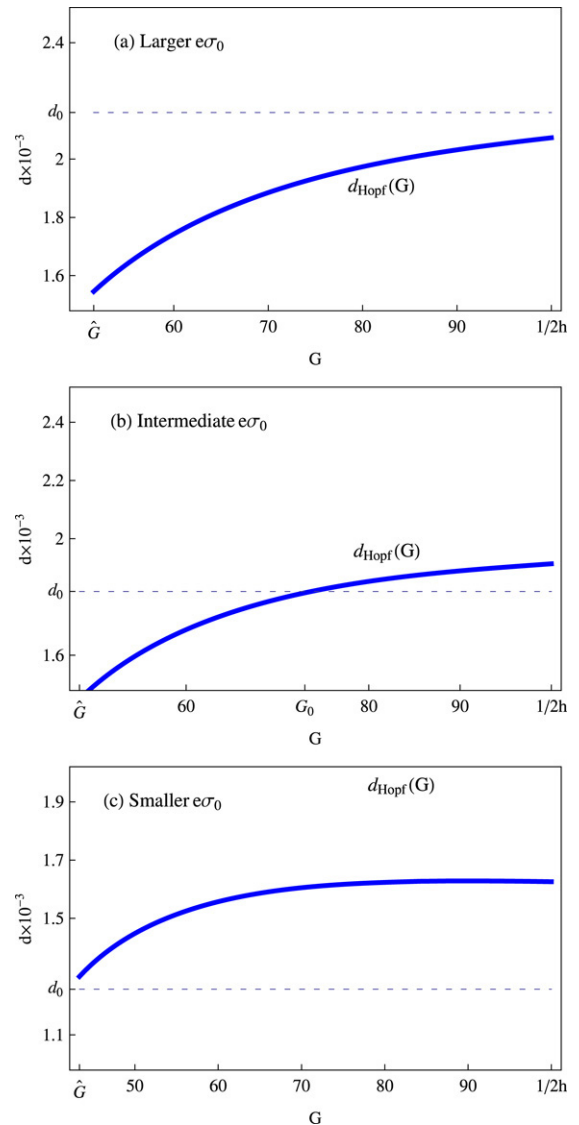
Fig. 6. Diagram showing how the position of the Hopf bifurcation (d_{Hopf}) varies with G in Case 1, compared with where it occurs (d_c) for the same parameters of the Holling Type 2 functional response in the absence of a toxicant effect. Three different values of $e\sigma_0$ are used; (a) 0.00025, (b) 0.00023, and (c) 0.00019. Other parameter values are: $r = 0.01$, $K = 1\,700\,000$, $h = 1/200$, and $B = 0.00003$.

Case 2. Again, for $G < G_c$ on the G-axis ($w = 0$), there is an equilibrium point. This is because $w = BG - d = 0$ along this axis, and $C(N)$ reaches a maximum of G at $N = N_m$, where $N_m < K$. Therefore, one equilibrium point is possible. Recall that in Case 1 there is no descending limb on the right-hand side of $C(N)$ ($N^* > N_m$), so that, for $G < G_c$, if d was decreased so that $w > 0$, there was still only one equilibrium. Now, for Case 2, where a descending limb is possible, we can see that when $G < G_c$ (so that $N_m < K$) and d is decreased slightly, there are two possible equilibria. This is best seen in Fig. 8, where various positions of the line d/B are shown intersecting with the functional response curve $C(N)$. As d decreases further [we move in the positive w-direction of the (G, w) bifurcation plane (Fig. 9)], the equilibrium corresponding to the descending limb will ultimately disappear, because the point
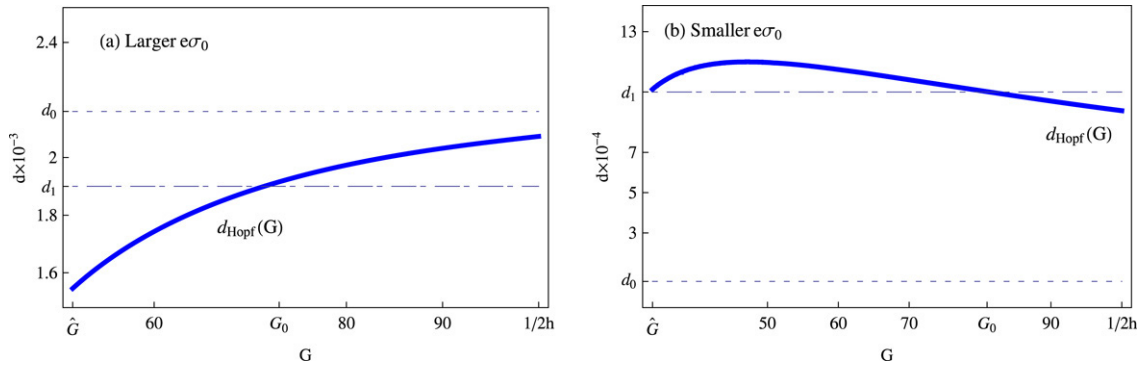
Fig. 7. Diagram showing how the position of the Hopf bifurcation (d_{Hopf}) varies with G in Case 1, compared with where it occurs (d_c) for the same parameters of the Holling Type 2 functional response in the absence of a toxicant effect. (a) $e\sigma_0 = 0.00025$, and (b) $e\sigma_0 = 0.00012$. Other parameter values are as in Fig. 6.

of intersection of d/B and $C(N)$ will at some point exceed K (see Fig. 8). The dividing line between one and two interior equilibria is represented by the part of the $w_K(G)$ curve to the left of G_c, which was equal to 0 in Case 1 (see the broken line along G-axis is Fig. 3). This $w_K(G)$ curve forms a new dividing line between Regions I and III (see Fig. 9).

The two interior equilibria $E_i^* = (N_i^*, P_i^*)$ ($i = 1, 2$) satisfy the equations

$$BC(N) = d \quad \text{and} \quad P = g(N) \tag{23}$$

with $0 < N^* < K$. Solving the first equation in Eq. (23) for N, we get the following quadratic equation:

$$a_2 N^2 + a_1 N + a_0 = 0,$$

where

$$a_0 = -dG, \qquad a_1 = e\sigma_0 G(B - 2hd),$$
$$a_2 = e^2\sigma_0^2(BhG - B/4 - dh^2G).$$

Solutions are shown in Appendix 3 in the online version of this paper. In particular, it can be shown that there are now two possible solutions, or two possible interior equilibria, N_1^* and N_2^*. To repeat, this simply reflects the fact that $C(N)$, unlike $C_1(N)$, is unimodal.

We can examine the nature of the solutions of Eq. (23) (and consequently the corresponding equilibria) on the bifurcation plane (Fig. 9). As mentioned above, in order to form biologically meaningful interior equilibria, the two solutions N_1^* and N_2^* need to satisfy the conditions $0 < N_1^*, N_2^* < K$. Notice from Eq. (21) that N_1^* and N_2^* are intersections of the curve $C(N)$ and the horizontal line d/B (see Fig. 8). Since $N(t) \leq K$ and $C(N)$ assumes its maximum value, G, at N_m (see Fig. 8), the number of intersection points can be either two, or one, or none. The curve $w_K(G)$ determines the nature of the interior equilibria. More specifically, from the examination of Fig. 8, the following two properties hold:

(P1): If $N_m < K$, then the line d/B intersects with the curve $C(N)$ at two points, N_1^* and N_2^*. These are both less than K, if $w < w_K$, but the line d/B intersects with the curve $C(N)$ at only one point less than K, N_1^*, for $w \geq w_K$. Thus there are two interior equilibria $E_i^* = (N_i^*, P_i^*)$ if $w < w_K$ and only one if $w \geq w_K$. The two equilibria are, (1) the original equilibrium, E_1^* from Case 1, which can be either stable or
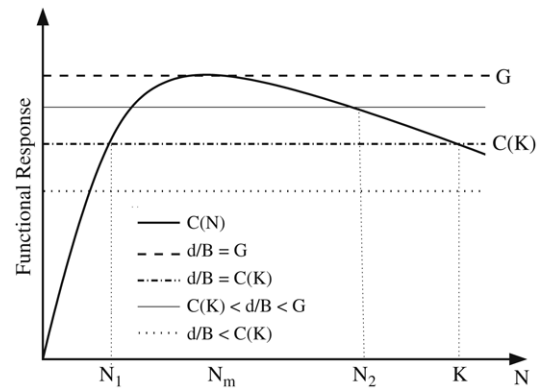
Fig. 8. The N^* component of an interior equilibrium is shown as an intersection of the curve $C(N)$ with a horizontal line d/B. If d/B is between the values of $C(K)$ and G, then there are two intersections, N_1^* and N_2^* in $(0, K)$, corresponding to two interior equilibria. If d/B is smaller than $C(K)$ then there is only one intersection N_1^* in $(0, K)$ (not labeled), corresponding to the unique interior equilibrium.

unstable, and a new one, E_2^*, which is a saddle point. The saddle point is unstable, and can lead to extinction of the herbivore, so its existence represents danger to the herbivore. If d is small enough, however, the d/B line is lower than the $C(K)$ line in Fig. 8, which means that the herbivore is much safer from extinction.

(P2) If $N_m > K$, then the line d/B intersects with the curve $C(N)$ at only one point, N_1^*, for $w \geq w_K$, and there is no intersection for $w < w_K$.

Summarizing the results, we can divide the region of interest in the (G, w)-plane into three subregions.

I. In this region the unique interior equilibrium is either $E_1^* = (N_1^*, P_1^*)$ (in this case $N_2^* > K$) or $E_2^* = (N_2^*, P_2^*)$ (in this case $N_1^* \leq 0$).
II. In this region there is no interior equilibrium.
III. In this region, two equilibria exist, $E_i^* = (N_i^*, P_i^*)$ ($i = 1, 2$) ($0 < N_1^* < N_2^* < K$).

The locations of the interior equilibria in these regions are depicted in Fig. 9.

2.3.2. Stability of equilibria and Hopf bifurcation

At an interior equilibrium $E^* = (N^*, P^*)$, where N^* and P^* satisfy the same equations as given in Eq. (23), the Jacobian
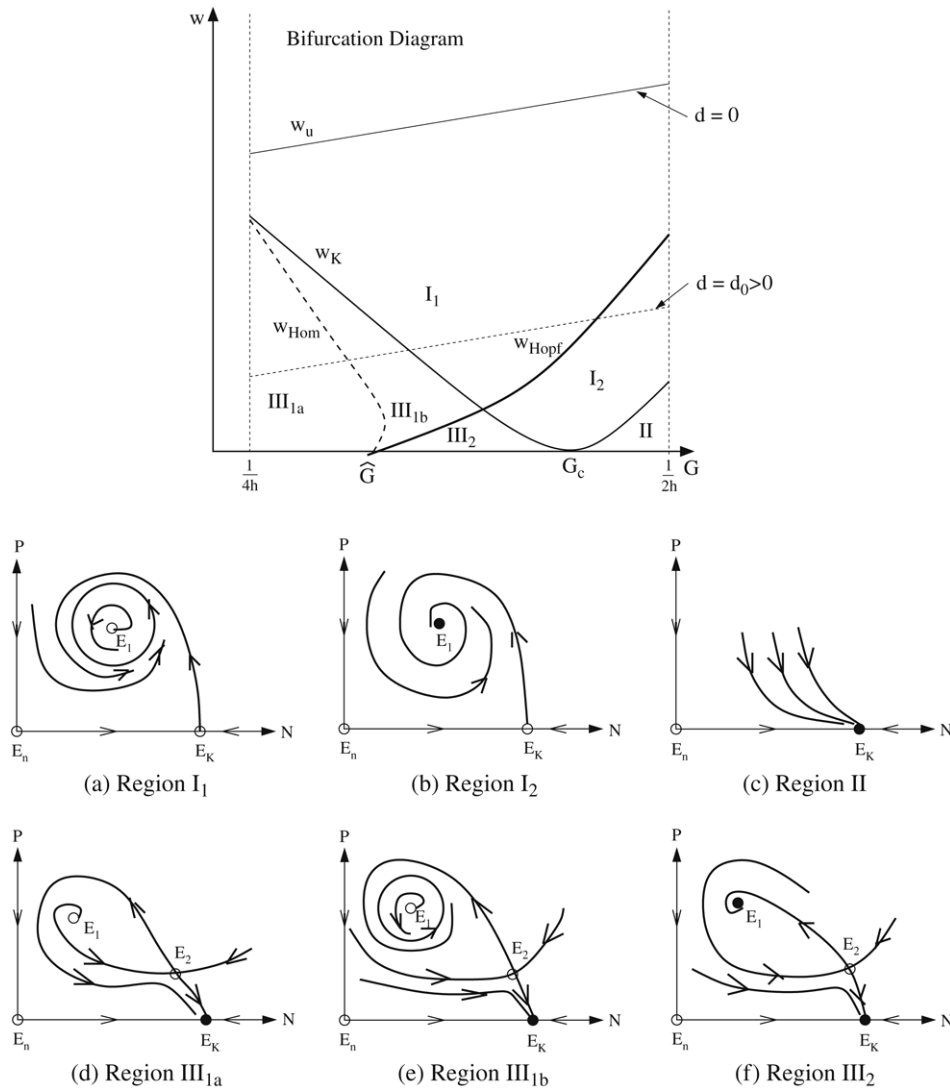
Fig. 9. The top panel shows the bifurcation diagram for Case 2, where $\sigma = \sigma_0$ (constant). The axes are G and $w = BG - d$. The bottom panels (a)–(f) are the sketches of phase portraits for (G, w) in various regions. See the text for explanation. The parameter values used are the same as in Fig. 3.

matrix is the same as that given in Eq. (20). The interior equilibrium E_2^* is always a saddle whenever it exists, since $g'(N_2^*) > 0$. Setting $g'(N_1^*) = 0$, together with $BC(N_1^*) - d = 0$, we can obtain the same Hopf bifurcation curve, $w = w_{\text{Hopf}}(G)$ as given in Case 1, such that the interior equilibrium E_1^* is stable for $w < w_{\text{Hopf}}$ and unstable for $w > w_{\text{Hopf}}$. A more detailed proof of this result can be found in Liu et al. (in press). It can be checked that the two curves, $w_{\text{Hopf}}(G)$ and $w_K(G)$ intersect at only one point, and that $w_{\text{Hopf}}(G)$ is increasing, lies below the line $w_u(G)$ for all $\hat{G} \le G \le 1/2h$, and intersects the w-axis at $\hat{G}$. Using the above information we know that the curve $w_{\text{Hopf}}(G)$ is as shown in the bifurcation diagram Fig. 9. The curve $w_{\text{Hopf}}(G)$ divides Region I into regions I_1 and I_2 and divides Region III into regions III_1 ($=III_{1a} \cup III_{1b}$) and III_2. Results for the stability of equilibria in these regions are summarized in Table 3.

Notice that a saddle-node bifurcation occurs along the G-axis, or $w = 0$ line (so as w increases from 0 the single equilibrium divides into a saddle point and a node) and a

Table 3
Local stability results when σ is constant

	I_1	I_2	II	III_{1a}	III_{1b}	III_2
E_0	Saddle	Saddle	Saddle	Saddle	Saddle	Saddle
E_1^*	Unstable	**Stable**	DNE	Unstable	Unstable	**Stable**
E_2^*	DNE	DNE	DNE	DNE	Saddle	Saddle
E_K	Saddle	Saddle	**Stable**	**Stable**	**Stable**	**Stable**
PS	**Stable**	DNE	DNE	DNE	**Stable**	DNE

DNE: Does not exist; PS: Periodic solution.

Hopf bifurcation occurs along the curve $w_{\text{Hopf}}(G)$. The curve $w = w_{\text{Hopf}}(G)$ intersects $w = 0$ at the point $(\hat{G}, 0)$, which is a cusp point of co-dimension 2, implying the possibility of a homoclinic bifurcation (discussed in more detail in Liu et al. (in press); see also Appendix 4 in the online version of this paper). The homoclinic curve $w = w_{Hom}(G)$ is shown in Fig. 9, which further divides Region III_1 into two subregions, III_{1a} and III_{1b}. The corresponding phase portraits in these regions are depicted in Fig. 9(a)–(f). We remark that, although the above analytic

results are only for local stability analysis, Fig. 9(a)–(f) actually illustrate global bifurcation diagrams and show how the local phase portraits of various equilibria may be connected.

To verify the above analytic results, numerical simulations were performed for the system (Eqs. (10a)–(10c)). These are shown in Appendix 5 in the online version of this paper.

As in Case 1, we can attempt to interpret ecologically the features of the new bifurcation diagram (Fig. 9). Again, we decrease both G and w, but keep d fixed ($d = d_0$), along a diagonal straight line from the middle-right-hand corner of the bifurcation diagram (Fig. 9) towards the lower-left-hand corner, then we can see the effects of G alone on the system behavior. The system undergoes a series of changes leading from dominance of simple Holling Type II dynamics to dominance by the effect of the toxicant. As G and w decrease, moving from Region I_2 to I_1, the single stable interior point, $E_1^* = (N_1^*, P_1^*)$, becomes unstable, producing a limit cycle, a result of increasing toxicant effect. As G and w continue to decrease and move into Region III_{1b}, the saddle point moves into the positive quadrant, with $N_2^* < K$, so there are now two interior equilibria. Biologically, the behavior for decreasing G means that in this region of parameter space the individual herbivores may have trouble dealing with the amount of toxicant that they are ingesting, and the possibility exists of the herbivore being in an alternative state of poor physiological condition; the saddle point $E_2^* = (N_2^*, P_2^*)$. The limit cycle around the point E_1^* can be changed to a stable node by holding G fixed and decreasing w into Region III_2. In Region III the consumer population is in some danger of going to extinction due to the toxicant ingested from the plant, because the herbivore has no control over its rate of ingestion, which is completely determined by the density of plant food items, N. The fate of the herbivore population depends on the initial values of N and P. If N starts at a large value, then, because the herbivore feeding rate increases with plant density, the herbivores' consumption will drive them to extinction and the system will approach the boundary equilibrium $N = K$, $P = 0$. Also, even if N is initially small, but P also starts out very small, the herbivore may ultimately go to extinction. This is because an initially small value of P allows N to grow long enough to reach density levels that lead to the herbivore population dying out from toxicity. A relatively small initial value of N, together with relatively large P, however, could allow the system to be captured by the stable limit cycle around E_1^*.

Further decreases in G and w from Region III_{1b} take the system across the homoclinic threshold into Region III_{1a}. In this region, the limit cycle is close enough to the saddle that it is no longer possible for a stable limit cycle to exist, as it is 'captured' by the saddle point. Now trajectories from every point in the (N, P)-plane lead towards the saddle point and ultimately to the boundary point $E = (K, 0)$, where the herbivore is extinct. Ecologically this means that the level of toxicant in the plant is so high that the herbivore cannot survive on the plant. It can obtain enough energy from the plant to survive only at the cost of absorbing so much toxicant that it dies.

3. Discussion

This paper analyzes the equilibria and dynamics of a toxicant-determined functional response using bifurcation diagrams. Without the multiplicative factor representing toxicant effect in Eq. (1), this model would reduce to the RM model (Eqs. (7a) and (7b)); i.e., $C(N)$ reduces to $f(N)$. Our study is limited to one resource, or plant type, of the herbivore, so the effects of alternative diets are not possible in this model. The herbivore has only two choices. In Case 1 it can reduce its feeding rate when the density of resources exceeds the density N_m, and thus prevent declining growth due to physiological damage from the toxin. In Case 2 the herbivore continues to eat beyond the rate at which it experiences harm from the toxicant. In this case, it does not behaviorally limit intake. However, when food density exceeds N_m, the toxic effects of the food will put the herbivore in a physiological state in which its ingestion decreases to a lower level.

In Case 1 the qualitative dynamics of the herbivore-plant system are changed somewhat from the RM model. Decreasing the value of G, while d is held constant (meaning that the effects are due to the toxicant alone) lowers the rate of ingestion of food, and viability of the consumer becomes completely impossible for $G < 1/4h$. The toxicant also has an effect on the stability, shifting the value of d at which a Hopf bifurcation occurs. In Appendix 6 in the online version of this paper we both offer a justification of the TDFRM and show that, for relatively large values of G, the effect of decreasing G is very similar in effect to increasing the herbivore's handling time of plant resources. Therefore, just as an increase in handling time, h, in the RM model often decreases the d_c of the Hopf bifurcation (that is, it is stabilizing) (see Eq. (9)), a decrease in G can decrease d_{Hopf} (or be stabilizing, as in Fig. 7(a)). However, we also observed that decreasing G can be destabilizing (Figs. 3 and 7(b)). This occurs for larger values of $e\sigma_0$ and again is consistent with what happens in the RM model for large values of $e\sigma_0$ (such that $he\sigma_0 K \approx> 1$). In that case an increase in h leads to an increase in d_c in the RM model. We show in Appendix 6 in the online version of this paper that decreasing G in the TDFRM has the same qualitative effect as increasing h in the RM or TDFRM. For all $G < \hat{G}$ the interior equilibrium point is always unstable in the (G, w)-plane. Decreasing values of G are also shown to cause a rapid increase in the period of the limit cycle (Appendix 3 in the online version of this paper). This appears to result from the slow recovery of the herbivore from population declines, and indicates that herbivore cycles may be longer when plants are heavily defended by chemicals.

Research on herbivores indicates that aversion of toxic plants (conditioned food aversions) can occur in large domestic animals (Provenza et al., 2003), and has been indicated for other herbivores as well. However, the possibility of continued feeding on toxic resources to the point at which negative effects occur should be considered, at least, possible. In Case 2, in which this is allowed to happen, the qualitative behavior of the plant–herbivore interaction is drastically changed. Now there is the possibility of two interior equilibria. One state is the healthy state in which $N = N_1^*$ is low enough that the herbivore's food

intake is below its peak level In this state herbivore grazing exerts a top–down effect, controlling the plant biomass down to this level. The other equilibrium, at a higher plant biomass level, N_2^*, represents a weakened state of the herbivore with a smaller population value. In this state the herbivore density is depressed, as it is controlled by the plant defenses. Its ingestion rate is decreased because of physiological damage from the toxin. The herbivore population is not trapped in that state, because E_2^* is a saddle point (unstable). A slight decrease in N would produce positive feedback mechanisms taking the herbivore back to E_1^*, either a stable equilibrium or stable limit cycle. But a slight increase in N would push the herbivore population in the opposite direction, towards extinction.

Although our model considers only fixed chemical defenses of the plant, it can be compared with a model of induced defenses (Edelstein-Keshet and Rausher, 1989), which also predicts a depression of herbivore density due to plant defenses. Those authors modeled herbivore per capita growth rate as $r_0(1 - \bar{Q}/q_c)$, where $\bar{Q}$ is the average level of plant defenses, q_c is the critical level of defenses at which the herbivore growth rate goes to zero, and r_0 is the herbivore growth rate in the absence of defenses. The authors also found that, unlike our two model cases, only under unusual conditions did persistent fluctuations arise. However, their model differs from ours in that herbivore growth depends only on plant quality, not quantity, and that the defenses are induced. More recently, Vos et al. (2004) also found that a predator–prey interaction with inducible defenses may be more stable than one with fixed defenses.

Only one food source is considered in the TDFRM, so while the model demonstrates that strong selective pressure should occur for food aversion, the model does not include the possibility of selection among a variety of food choices, which have varying degrees of toxins of different types. As has been noted (e.g., Dearing et al. (2005)) many terrestrial herbivores feed on a variety of plants to reduce the impact of any given toxicant. Kent et al. (2005) have shown that variations in feeding between preferred and non-preferred prey can result in cycles similar to real cycles. In particular, they noted that the lengthening of the periods of microtine cycles from south to north may be a result of slower recovery of favored plant species as a function of latitude. Our model predicts cycles that increase in period with strength of toxicant effects. However, we agree that rigorous study of herbivore cycles requires consideration of multiple resource species. The TDFRM model presented here is capable of being extended to multiple plant species and multiple herbivores. One of the uses to which the model will be put in the future is to examine coexistence of plant and herbivore species when not only the parameters of life history and trophic interaction but also parameters for plant toxicant production and herbivore ability to tolerate toxicants differ among species.

Acknowledgments

Appendix. Supplementary data

Supplementary data associated with this article can be found, in the online version, at doi:10.1016/j.tpb.2007.12.004.

References

Abrams, P.A., 1989. Decreasing functional responses as a result of adaptive consumer behavior. Evol. Eco. Res 3, 95–114.

Bryant, J.P., Chapin III, F.S., Klein, D.R., 1983. Carbon/nutrient balance of boreal plants in relation to herbivory. Oikos 40, 357–368.

Bryant, J.P., Provenza, F., Reichardt, P.B., Clausen, T.P., 1992. Mammal-woody plant interactions. In: Rosenthal, G.A., Berenbaum, M. (Eds.), Herbivores: Their Interaction with Plant Secondary Metabolites, vol. 2. Academic Press, New York, NY.

Bryant, J.P., Swihart, R.K., Reichardt, P.B., Newton, L., 1994. Biogeography of woody chemical defense against snowshoe hare browsing: Comparison of Alaska and eastern North America. Oikos 70, 385–394.

Coley, P.D., Bryant, J.P., Chapin III, F.S., 1985. Resource availability and plant antiherbivore defense. Science 230, 895–899.

Dearing, M.D., Foley, W.J., McLean, S., 2005. The influence of plant secondary metabolites on the nutritional ecology of herbivorous terrestrial vertebrates. Annu. Rev. Ecol. Evol. Syst. 36, 169–189.

Edelstein-Keshet, L., Rausher, M.D., 1989. The effects of inducible plant defenses on herbivore populations. 1. Mobile herbivores in continuous time. Am. Nat. 133, 787–810.

Holling, C.S., 1959a. The components of predation as revealed by a study of small mammal predation on the European sawfly. Can. Ent. 91, 293–320.

Holling, C.S., 1959b. Some characteristics of simple types of predation and parasitism. Can. Ent. 91, 385–398.

Kent, A., Jensen, S.P., Doncaster, C.P., 2005. Model of microtine cycles caused by lethal toxins in non-preferred food plants. J. Theoret. Biol. 234, 593–604.

Li, Y., Feng, Z., Swihart, R., Bryant, J., Huntley, H., 2006. Modeling plant toxicity on plant-herbivore dynamics. J. Dynam. Differential Equations 18 (4), 1021–1024.

Liu, R., Feng, Z., Zhu, H., DeAngelis, D.L., 2008. Bifurcation analysis of a plant-herbivore model with toxin-determined functional response. J. Differential Equations (in press).

Lundberg, P., 1988. Functional response of a small mammalian herbivore: The disc equation revisited. J. Anim. Ecol. 57, 999–1006.

Lundberg, P., Astrom, M., 1990. Low nutritive quality as defence against optimally foraging animals. Am. Nat. 135 (4), 547–562.

Marsh, K.J., Wallis, I.R., Foley, W.J., 2007. Behavioral contributions to the regulated intake of plant secondary metabolites in koalas. Oecologia 154 (2), 283–290.

Murdoch, W.W., 1966. Community structure, population control, and competition: A critique. Am. Nat. 100, 219–226.

Palo, R.T., Robbins, C.T., 1991. Plant Chemical Defenses Against Mammalian Herbivory. CRC Press, Boca Raton, Florida.

Provenza, F.D., Villalba, J.J., Dziba, L.E., Atwood, S.B., Banner, R.E., 2003. Linking herbivore experience, varied diets, and plant biochemical diversity. Small Rum. Res. 49, 257–274.

Rosenthal, G.A., Berenbaum, M. (Eds.), 1992. Herbivores: Their Interaction with Plant Secondary Metabolites, vol. 2. Academic Press, New York, New York.

Rosenzweig, M.L., 1971. Paradox of enrichment: Destabilization of exploitation ecosystems in ecological time. Science 171, 385–387.

Spalinger, D.E., Hanley, T.A., Robbins, C.T., 1988. Analysis of the functional response in the Sitka black-tailed deer. Ecology 69, 1166–1175.

Terborgh, J., et al., 2006. Vegetation dynamics of predator-free land-bridge islands. J. Ecol. 94 (2), 253–263.

Villalba, J.J., Provenza, F.D., Bryant, J.P., 2002. Consequences of nutrient-toxin interactions for herbivore selectivity: Benefits of detriments for plants? Oikos 97, 282–292.

Vos, M., Kooi, B.W., DeAngelis, D.L., Mooij, W.M., 2004. Inducible defences and the paradox of enrichment. Oikos 105, 471–480.